A Research on the Impact of 20 mm × 102 mm Armor-Piercing Frangible Projectiles on Multilayer Armor

Mihaela Badea
National Politehnica University of Science and Technology, Bucharest, Romania
radu.cristianamihaela@gmail.com

Dragos Gabriel Zisopol
Department of Mechanical Engineering, University of Petroleum and Gas, Ploiesti, Romania
zisopold@upg-ploiesti.ro (corresponding author)

Vasile Nastasescu
"Ferdinand I" Military Technical Academy, Bucharest, Romania
nastasescuv@gmail.com

Anton Hadar
National Politehnica University of Science and Technology, Bucharest, Romania
anton.hadar@upb.ro

Received: 26 June 2025 | Revised: 28 July 2025 | Accepted: 3 August 2025

Licensed under a CC-BY 4.0 license | Copyright (c) by the authors | *DOI: https://doi.org/10.48084/etasr.12971*

ABSTRACT

The current paper investigates the impact of 20 mm × 102 mm frangible armor-piercing projectiles on multilayer armor, specifically of land-based systems. The novelty and aim of the present research were to analyze, through both numerical and experimental methods, the behavior of the 20 mm × 102 mm frangible armor-piercing projectiles upon impact with multilayer armor, considering their unique design features. In addition to the experimental tests involving live firings in a dedicated testing range, numerous numerical simulations were conducted with various projectile models. Both 2D and 3D models considered an elasto-plastic model with kinematic hardening, suited of capturing the onset and progression of the material fracture, with a relatively small set of control parameters. The numerical results closely matched the experimental data, with error in the order of 1%.

Keywords-armor-piercing; frangible projectile; multilayer armor; material model; numerical model

I. INTRODUCTION

As new types of projectiles appear along with new types of armor, the need for periodic validation of ammunition and new methods and means of experimental and numerical investigation emerges [1-3]. The current work investigates the impact of a relatively new type of projectile (frangible projectile) on multilayer armor plates. The behavior of the 20 mm ×102 mm frangible armor-piercing projectile is studied both in the design process and operation, and especially after a certain period of storage. The research involves both experimental and numerical investigations [4]. The experimental research was carried out under normal standardized conditions, with modern equipment, which allowed both the recording of the impact phenomenon and the automatic determination for each case of the impact velocity and the remaining velocity. Numerical research was carried out using the finite element method [5, 6] in the facilities offered by the Ansys/Ls-Dyna program [7, 8]. Since the studied impact was the normal impact on flat armor plates, the problem to be studied was an axial-symmetrical one. Thus, axial-symmetric 2D finite element models were mainly used (substantially reducing computation time), along with reduced 3D models (a quarter of the structure) due to the existence of two planes of geometric and mechanical symmetry. A very important decision in the study was the choice of the material model. Mechanical engineering in general, and especially the Ansys/Ls-Dyna program provides the user with many material models, taking into account many phenomena specific to the projectile-armor impact (elasto-plastic behavior, phenomenon of consolidation beyond the yield point, friction, hourglass energy, different fracture (ductile or brittle) criteria, the effect

of temperature, etc.) [9, 10]. From the library of material models of the Ansys/Ls-Dyna program, the elasto-plastic material model was mainly used with kinematic consolidation (specific in the description of the material fracture), which uses the Cowper-Symond coefficients to describe the material behavior, whereas the moment of fracture is defined by the value of the specific deformation at damage or fracture [11]. It was also possible to consider, in addition to the widely known types of energy, the hourglass potential energy and the frictional energy. The good agreement of the numerical results with the experimental ones validates the accuracy of the finite element model used, of the modeling methodology, and of the adopted hypotheses, such as neglecting the thermal effects considering the ratio between the caliber of the projectile and the thickness of the armor plates [12-14]. The results of the research are presented in comparison with the experimental ones. The analyzed parameters were the impact velocity and the residual velocity. The results of this research are useful to both design and operation and testing stakeholders, in terms of the projectile and the armor plates.

II. MATERIALS AND METHODS

A critical decision during this study was the selection of the material model. Within mechanical engineering, and particularly in the Ansys/Ls-Dyna program, numerous material models are provided, allowing accurate representation of various materials while accounting for phenomena specific to projectile–armor impacts. These include elasto-plastic behavior, strain hardening beyond the yield point, friction, hourglass energy, fracture criteria (ductile or brittle), and temperature effects. From the Ansys/Ls-Dyna material model library, the elasto-plastic model with kinematic hardening was primarily adopted, as it is well suited for describing material fracture. In this model, Cowper–Symonds coefficients are used to characterize material behavior, and the fracture moment is defined by the value of specific strain at damage or breakage. In addition to the commonly recognized energy types, hourglass potential energy and frictional energy were also considered. The projectile components, numbered in Figure 1, are: 1-frangible hard (bullet) core, 2-bullet jacket, 3-bullet filler, 4-bullet cover, 5-bullet body, 6-the throwing explosive [2]. The properties of the FAP projectile component materials are presented in Table I.

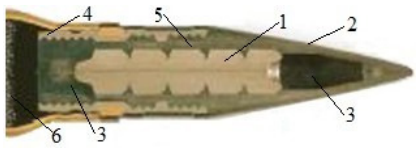

Fig. 1. The components of the FAP projectile.

TABLE I. PROJECTILE MATERIAL ELASTIC PROPERTIES

	Component materials	Young modulus (E) [Pa]	Poisson rate (v) [-]	Density (p) [kg/m^3]
1	Tungsten alloy	2.05×10^{11}	0.3	15450
2	Brass	1.38×10^{11}	0.33	8330
3	Filler	2.75×10^{9}	0.43	750
4	Steel	2.1×10^{11}	0.3	7850
5	Aluminum	0.70×10^{11}	0.34	2700

Figure 2 and Table II schematically present those three target variants and the respective layer size. The elastic characteristics of the materials of the component plates of the multilayer armor are presented in Table III.

Fig. 2. The three variants of the multilayer targets.

TABLE II. TARGET CONFIGURATIONS

Target dimensions	Construction variants		
	v-1	v-2	v-3
	Steel and aluminum	Steel, aluminum, and plastics	Steel and plastics
Height [mm]	250	250	250
Width [mm]	250	250	250
Thickness [mm]	14 + 9	14 + 5 + 4	14 + 9

TABLE III. TARGET MATERIAL ELASTIC PROPERTIES

Materials	Young modulus (E) [Pa]	Poisson rate (v) [-]	Density (p) [kg/m^3]
Steel	2×10^{11}	0.27	7865
Aluminum	0.7×10^{11}	0.34	2730
Plastics	3.04×10^{9}	0.42	6173

In the conducted research the experimental method and the numerical method were used.

III. EXPERIMENTAL METHOD

The experimental research was conducted through live firings at a specialized ammunition testing range, randomly selecting tests from a batch. The firing was performed using the M461 ballistic cannon and the ammunition, which is a 20 mm × 102 mm FAP [2]. The armor plates (targets) were secured in a custom-designed device specifically made for these experiments. To measure and record impact parameters such as impact velocity, residual velocity, frame rate, and distance, specialized equipment was used, including a dedicated software program and a PHOTRON FASTCAM SA-Z ultra-fast video camera. For each shot, the results were automatically displayed, along with measurements of the perforation size on both the front and back sides [2]. The impact velocities for the three target variants were 947.486 m/s, 1076.56 m/s, and 1036.96 m/s, respectively. Impact and residual velocities were automatically recorded by the equipment as shown in Table IV.

IV. NUMERICAL METHOD

The numerical method used was the finite element method, using the Ansys/Ls-Dyna program. Since the research was carried out only for the normal impact case [18-20], both the 2D axially symmetric model and the simplified 3D model were used; the 3D models were built for a quarter of the structure, because it, in the case of a normal impact, has two symmetrical planes. The research also included a focus on sphere modeling [21-23]. Two models from [2] were analyzed. The first, referred to as the Real Model (RM), was a true geometric representation, which often posed geometric challenges and was sometimes limited by inaccessible data. The second, referred to as the Equivalent Model (EM), was a simplified geometric representation that preserved the overall shape and weight. In this model, only the hard core was assigned a fictitious density to match the actual total weight. Figure 5 shows the 2D finite element models (Figures 5(a) and 5(b)) and the 3D finite element models (Figures 5(c) and 5(d)) of these configurations. In all cases, the projectile mass was maintained at 105 ± 1 g.

Fig. 3. 2D axisymmetric model, for target v-1.

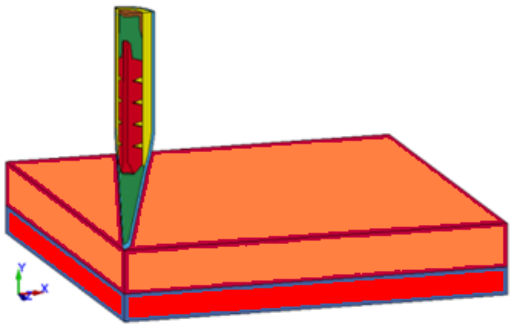

Fig. 4. Simplified 3D model for target v-1.

For the 2D models of the projectile, axisymmetric finite elements with four nodes and two degrees of freedom per node were used, while for the 3D models, solid brick elements with eight nodes and degrees of freedom per node from the Ls-Dyna program library were employed. The finite element dimensions vary between 0.5 mm and 2 mm. Figure 6 and Figure 7 display the 2D and 3D finite element models for target v-2. The finite element sizes range from 0.2 mm to 2 mm. A comparative presentation is provided in Tables IV and V.

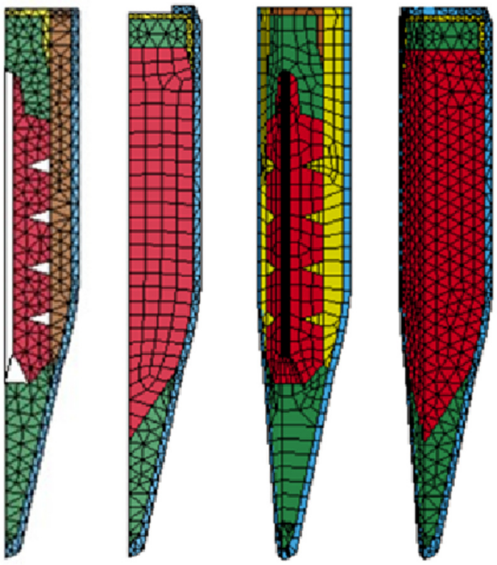

(a) (b) (c) (d)

Fig. 5. Finite element models of FAP 20 mm × 102 mm.

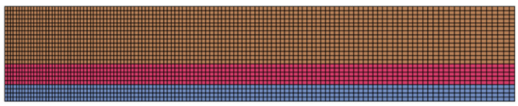

Fig. 6. 2D finite element model of target v-2.

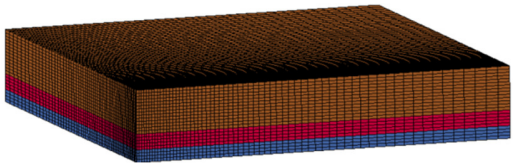

Fig. 7. 3D finite element model of target v-2.

Regarding the finite element modeling of the target, as seen in Figures 6 and 7, a non-uniform discretization was used. In the impact zone, the finite element size was 0.2 mm. In the numerical analysis performed, in both 2D and 3D models, the adopted material model was the plastic-kinematic one, called MAT_003 from the material library of software Ls-Dyna, both for projectile and armor plates modeling. The values of Cowper Symonds coefficients (C and P) were 40 and 5 for steel and 6500 and 4 for tungsten alloy and aluminum, respectively.

V. RESULTS

The results of the experimental research are summarized in Table IV. In Table V, the results of the numerical research are presented in comparison with those of the experimental research. This comparison enhances credibility, emphasizes the novelty of the research, and offers valid approaches for similar problems.

TABLE IV. EXPERIMENTAL RESULTS

Target construction variants	Impact velocity [m/s]	Residual velocity [m/s]	Maximum diameter of the hole [mm]	
			Impact face	Back face
v-1	947.486	710.615	24	23
v-2	1076.56	662.5	22	21
v-3	1036.96	691.304	25	24

TABLE V. RESULT COMPARISON

Projectile models	Target variant	Impact parameters		
		Residual velocity (experiment)	Residual velocity (FEM)	Error percentage
		[m/s]	[m/s]	[%]
1	v-1	710.615	711	-0.05
	v-2	662.5	655	-1.13
	v-3	691.304	705	1.98
2	v-1	710.615	692	-2.62
	v-2	662.5	641	-3.25
	v-3	691.304	699	1.11

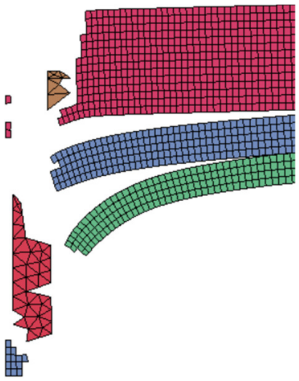

Fig. 8. Deformed state of the 2D projectile model 1- target v-2.

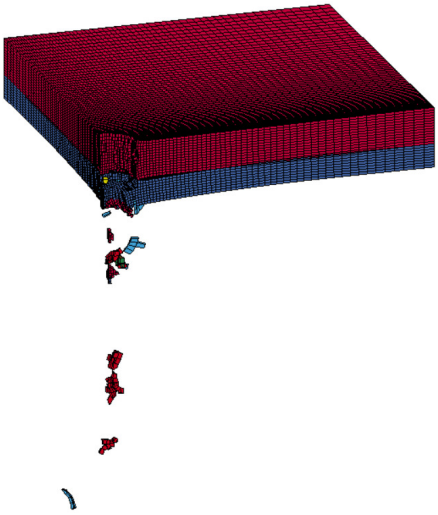

Fig. 9. Deformed state of the 3D projectile model 1- target v-1.

The errors presented in Table V indicate a very close agreement between the numerical and the experimental results for both projectile models. This confirms the validity of using the equivalent projectile (Model 2). The use of projectile Model 1 also made it possible to clearly observe the fragmentation of the hard core, as shown in Figures 8 and 9 for the 2D and 3D models, respectively [24]. Figures 10-15 present the curves showing projectile velocity variation during penetration. In all cases, the targets were fully perforated, and the numerically calculated residual velocities showed very close agreement with the experimentally measured values. Figure 16 shows the projectile velocity variation curve during penetration in the case of 3D modeling, with projectile model 1 and target v-1. The error between the numerical value and the experimental one is only 0.37%.

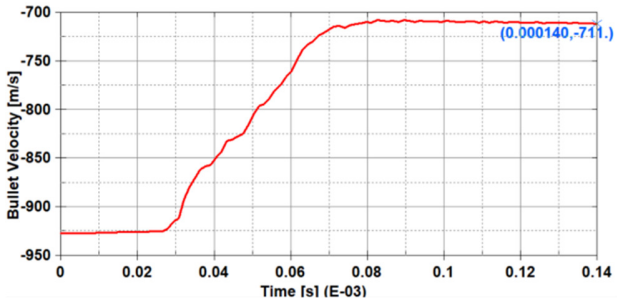

Fig. 10. Time evolution of projectile 1 in target v-1.

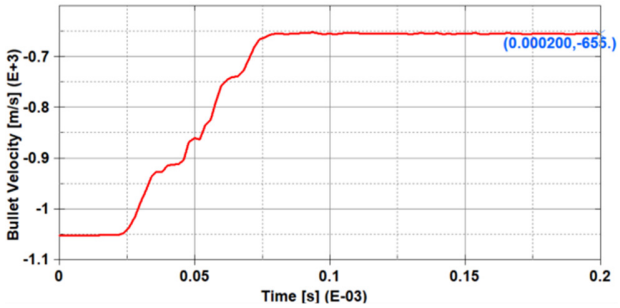

Fig. 11. Time evolution of projectile 1 in target v-2.

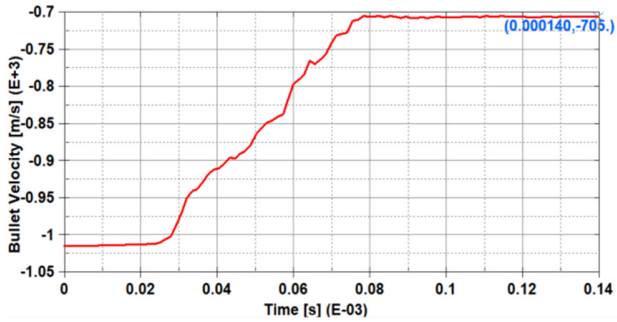

Fig. 12. Time evolution of projectile 1 in target v-3.

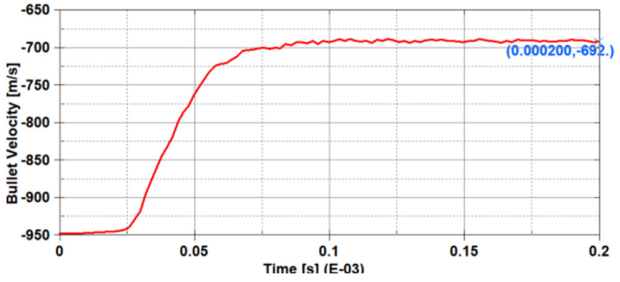

Fig. 13. Time evolution of projectile 2 in target v-1.

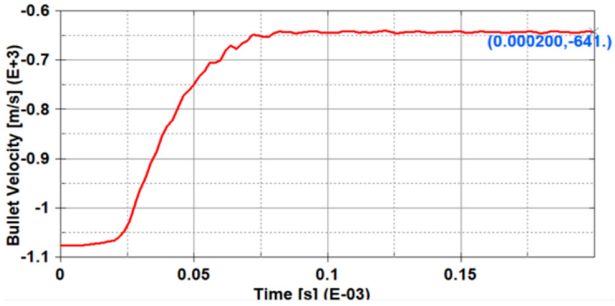

Fig. 14. Time evolution of projectile 2 in target v-2.

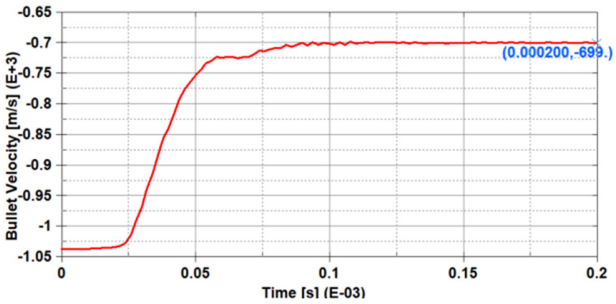

Fig. 15. Time evolution of projectile 2 in target v-3.

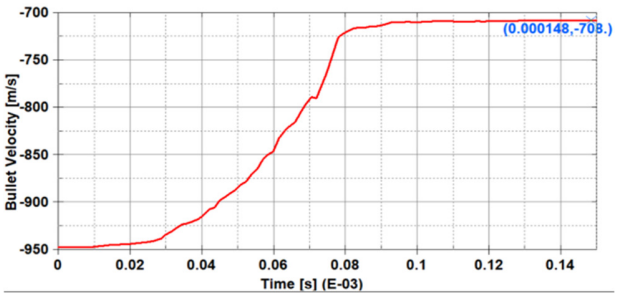

Fig. 16. Time evolution of projectile 1 in target v-1, in 3D modeling.

VI. CONCLUSIONS

Both the experimental and numerical results of this study are in very good agreement, which validates the concepts, models, and methodology used. The novelty of this paper consists in introducing the concept of the equivalent bullet, eloquently represented by projectile Model 2, which can be used in both 2D and 3D modeling. The novelties in the paper are based on a comparative analysis of geometric modeling, finite element models, and results. This research demonstrates, through an effective comparative analysis, that the most accurate results (with errors below 1%) are achieved when the projectile is modeled as closely to reality as possible. The use of equivalent projectile models (Model 2) proves to be a valid approach, producing results very close to the experimental values (with error around 1% or less) while simplifying the modeling process and reducing computational time.

REFERENCES

[1] V. Oana-Elena, "20 mm Frangible Armour Piercing Projectile," *Military Technical Academy*, vol. 5, Art. no. 050141.

[2] M. Badea, D. G. Zisopol, A. Hadar, and V. Nastasescu, "The Penetration Capacity of a 20 x 102 mm Frangible Armor Piercing Projectile," *Engineering, Technology & Applied Science Research*, vol. 15, no. 3, pp. 22996–23001, Jun. 2025, https://doi.org/10.48084/etasr.10708.

[3] T. Børvik, M. Langseth, O. S. Hopperstad, and K. A. Malo, "Ballistic penetration of steel plates," *International Journal of Impact Engineering*, vol. 22, no. 9, pp. 855–886, Oct. 1999, https://doi.org/10.1016/S0734-743X(99)00011-1.

[4] N. Kılıç, S. Bedir, A. Erdik, B. Ekici, A. Taşdemirci, and M. Güden, "Ballistic behavior of high hardness perforated armor plates against 7.62 mm armor piercing projectile," *Materials & Design*, vol. 63, pp. 427–438, Nov. 2014, https://doi.org/10.1016/j.matdes.2014.06.030.

[5] K. Bathe, *Finite Element Procedures*. Prentice Hall, 1996.

[6] N. J. Bićanić, "The finite element method (6th edn) (Its Basic and Fundamentals by O. C. Zienkiewicz, R. L. Taylor and J. Z. Zhu, ISBN 07506-6320-0, \54.99, Solid and Structural Mechanics by O. C. Zienkiewicz and R. L. Taylor, ISBN 07506-6321-9, \47.99 and Fluid Dynamics by O. C. Zienkiewicz, R. L. Taylor and P. Nithiarasu, ISBN 07506-6322-7, $47.99), Elsevier Butterworth-Heinemann, Oxford, 2005," *International Journal for Numerical Methods in Engineering*, vol. 68, no. 10, pp. 1113–1114, 2006, https://doi.org/10.1002/nme.1760.

[7] LS-DYNA Theory Manual. ANSYS, 2025.

[8] *LS-DYNA KEYWORD USER'S MANUAL VOLUME I*. ANSYS, 2012.

[9] V. Narayanamurthy, C. L. Rao, and B. N. Rao, "Numerical Simulation of Ballistic Impact on Armour Plate with a Simple Plasticity Model," *Defence Science Journal*, vol. 64, no. 1, pp. 55–61, Jan. 2014, https://doi.org/10.14429/dsj.64.4521.

[10] G. I. Balan, D. G. Zisopol, A. Stefan, V. Nastasescu, and L. Grigore, "Study of the Injection of Secondary Air into the Intake Manifold of the Gas Turbine to Avoid the Compressor Surging Phenomenon," *Engineering, Technology & Applied Science Research*, vol. 14, no. 2, pp. 13248–13254, Apr. 2024, https://doi.org/10.48084/etasr.6927.

[11] R. Laible, *Ballistic Materials and Penetration Mechanics*. Elsevier, 2012.

[12] Z. Rosenberg and E. Dekel, *Terminal Ballistics*. Springer, 2012.

[13] G. Ben-Dor, A. Dubinsky, and T. Elperin, "Method of basic impactors for simplified modeling of penetration," *Engineering Fracture Mechanics*, vol. 76, no. 4, pp. 614–618, Mar. 2009, https://doi.org/10.1016/j.engfracmech.2008.10.007.

[14] A. Morka, B. Jackowska, and T. Niezgoda, "Numerical study of the shape effect in the ceramic based ballistic panels," *Journal of KONES*, vol. 16, no. 4, pp. 539–548, 2009.

[15] E. A. Flores-Johnson, M. Saleh, and L. Edwards, "Ballistic performance of multi-layered metallic plates impacted by a 7.62-mm APM2 projectile," *International Journal of Impact Engineering*, vol. 38, no. 12, pp. 1022–1032, Dec. 2011, https://doi.org/10.1016/j.ijimpeng.2011.08.005.

[16] R. G. O'Donnell, "An investigation of the fragmentation behaviour of impacted ceramics," *Journal of Materials Science Letters*, vol. 10, no. 12, pp. 685–688, Jan. 1991, https://doi.org/10.1007/BF00722768.

[17] B. P. Kneubuehl, *Ballistics: Theory and Practice*. Springer Nature, 2024.

[18] R. McCoy, *Modern Exterior Ballistics: The Launch and Flight Dynamics of Symmetric Projectiles*. Schiffer Military History, 1998.

[19] A. Malciu, C. Pupăză, C.-C. Puică, and I.-F. Pană, "Finite element model validation for a 14.5 mm armor piercing bullet impact on a multi-layered add-on armor plate," *MATEC Web of Conferences*, vol. 373, 2022, Art. no. 00038, https://doi.org/10.1051/matecconf/202237300038.

[20] P. P. Massaro, *The Ballistics Handbook: Factors Affecting Bullet Flight from Muzzle to Target*. S.l.: Gun Digest Books, 2024.

[21] O. Lynch, *The Science of Ballistics*. Clanrye International, 2018.

[22] P. P. Massaro, *Big Book of Ballistics*. Iola: Gun Digest Books, 2017.

[23] G. Klimi, *Exterior Ballistics: The Remarkable Methods*. Xlibris Corporation, 2014.

[24] "30mm Armor-Piercing Ammunition - Defense Update:," Jun. 02, 2006. https://defense-update.com/20060602_30mm-ap.html.